The Effect of a Liquid Isothermal Bath in the Threadline on the Structure and Properties of Poly(ethylene terephthalate) Fibers

GANG WU, QIANG ZHOU, JIUNN-YOW CHEN, JOSEPH F. HOTTER, PAUL A. TUCKER, and JOHN A. CUCULO*

Fiber & Polymer Science Program, College of Textiles, North Carolina State University, Raleigh, North Carolina 27695-8301

SYNOPSIS

The process of melt-spinning poly(ethylene terephthalate) (PET) filament at high speeds was modified through the inclusion of a liquid isothermal bath (LIB) in the spinline. A wide range of positions, temperatures, and depths associated with the operation of the LIB were utilized in this study. The structural characteristics and mechanical properties of the as-spun fibers were characterized by birefringence, wide-angle X-ray diffraction (WAXD), infrared spectroscopy, and tensile testing. Experimental results showed that the structure and mechanical properties of the as-spun fibers were significantly influenced by the LIB operating conditions. The as-spun fibers prepared under optimum LIB conditions exhibit high birefringence and excellent mechanical properties. Results suggest the development of a critical value of threadline stress that is determined primarily by LIB depth and take-up velocity. Below this critical value, raising of LIB temperature, LIB depth, and take-up velocity resulted in increases of the apparent crystallite size, sample crystallinity, and both the crystalline and amorphous orientation. As would be expected, the mechanical properties of the fiber samples were improved in a corresponding manner. Above this critical stress value, molecular chains in the amorphous phase are stretched tautly, but the crystal growth process is restricted, resulting in a decrease in crystallite size and crystallinity, as well as a continued increase in mechanical properties. The fiber properties were also found to be very responsive to the relative location of the LIB. A unique structure, believed never before obtained in a one-step high-speed PET melt-spinning process, has been achieved that combines high amorphous orientation, low crystallinity, and high tenacity. © 1995 John Wiley & Sons, Inc.

INTRODUCTION

A vast amount of effort has been expended by the synthetic fiber industry in the development of high-performance fibers from poly(ethylene terephthalate) (PET). A variety of processing methods has been attempted in this effort, such as two-step spin-draw processes,[1,2] high-speed spinning,[3,4] zone drawing/zone annealing,[5,6] solid-state extrusion,[7,8] and solution spinning.[9,10] Generally, however, in the commercial production processes of high-performance PET yarns, only the two-step spin-draw technique has been widely utilized.

A typical commercial spin-draw process consists of an initial low-speed spinning stage followed by an integrated drawing and heat-setting stage that is performed using a high-speed mechanical drawing apparatus. Filaments thus obtained exhibit high strength, high modulus, low elongation, and high radial uniformity. The mechanical technological requirements, however, are relatively complicated, and the cost is high. To improve process economics, there has been increased interest over the last 20 years in melt-spinning of uniform polymer filaments at higher spinning speed. Although both productivity and as-spun undrawn fiber properties are improved

* To whom correspondence should be addressed.

Journal of Applied Polymer Science, Vol. 55, 1275–1289 (1995)
 CCC 0021-8995/95/091275-15

with increasing take-up speed, conventional spinning at high speeds remains incapable of yielding a fiber produced in one step that has properties equivalent to those of the traditional two-step process fibers. Typical high-speed spun fibers exhibit lower tenacity, lower Young's modulus, and greater elongation when compared with conventionally produced, fully oriented fibers.[11] Furthermore, for fibers spun above a critical take-up speed, structural multiformity such as a skin–core variation may occur.[12] Therefore, an important question has been raised, i.e.: If the ultimate goal is the development of an ideal one-step process for producing highly oriented/high performance PET fibers from a direct melt spinning process, how does one determine the appropriate threadline modifications and the corresponding optimum operating conditions associated with those modifications?

It is well known that there are many processing parameters that may influence the development of fiber structure in the melt-spinning process. Almost all such parameters, however, can be translated into a temperature, tension, and residence time effect. A melt-spinning process essentially is a succession of polymer treatments using combinations of these three variables.[13] In our previous studies, it was proved that the above three variables can be effectively controlled by applying a liquid isothermal bath along the spinline.[14,15] The spinning dynamics were changed from a process controlled by inertia and air drag forces to one controlled by an imposed liquid frictional drag. Such high tensile stress developed in the liquid bath induces higher molecular orientation within the as-spun fibers. This article presents the results of continuing research based on our previous studies and centers around a comprehensive analysis of a series of as-spun fibers, prepared over a wide range of take-up speed, liquid bath position, depth, and temperature. The effects of these parameters on the structural features and mechanical properties of the resulting as-spun fibers have been investigated.

EXPERIMENTAL

Materials

A commercial high molecular weight poly(ethylene terephthalate) (PET) chip was used to prepare all of the fiber samples for which data are presented in this study. Intrinsic viscosity (IV) as measured in a 60/40 (wt %) mixture of phenol and tetrachloroethane is 0.97 dL/g. The viscosity-average molecular weight, M_v, calculated from the following equation,[16] is about 29,400 g/mol:

$$IV = 2.1 \times 10^{-4} M_v^{0.82}$$

PET chips were dried in a vacuum oven at 140°C for at least 14 h before being transferred to the extruder.

Fiber Spinning Procedure

Figure 1 shows a schematic representation of the melt-spinning equipment. Polymer chips were conveyed and melted by an extruder with a screw diameter of 25 mm. A round single-hole spinneret having a 0.6 mm exit diameter, a spinning temperature of 300°C, and a throughput setup value corresponding to approximately a 4.5 denier as-spun filament product were used. A heated sleeve 5 cm long was installed near the spinneret face and the temperature of the sleeve was maintained at 290°C. No cross-flow or radial quench chamber was used

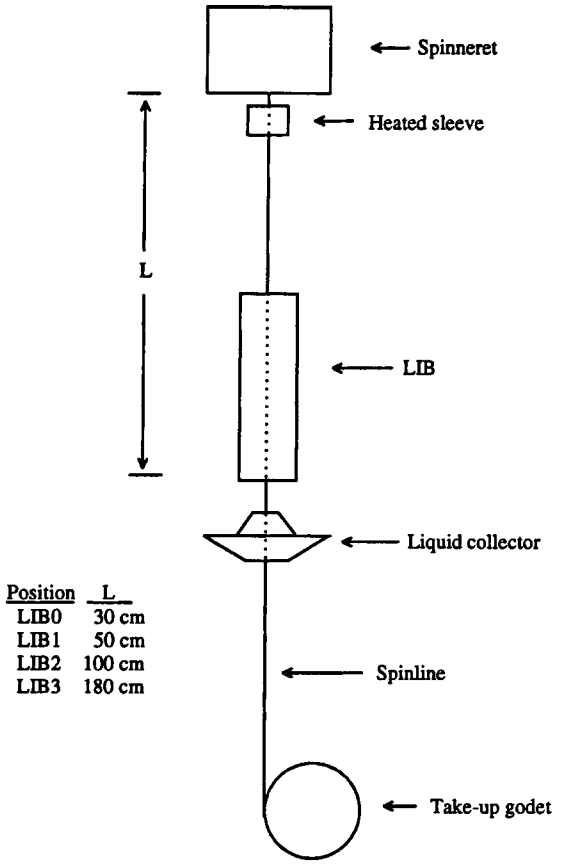

Figure 1 Schematic diagram of melt-spinning process with the liquid isothermal bath at four different positions.

in this study, although some degree of natural cooling must occur between the spinneret and the liquid isothermal bath (LIB).

The dynamic threadline modification was accomplished through the use of an LIB. The LIB could be moved along the spinline and was placed at each of the positions shown in Figure 1. The LIB position was varied such that the bottom of the bath was located at distances of 30, 50, 100, and 180 cm from the spinneret face, with each of these positions being designated in the following manner: LIB 0, LIB 1, LIB 2, and LIB 3, respectively. For each case, the distance from the spinneret face to the top surface of the liquid will be equal to the difference between the position of the bottom of the bath and the liquid depth.

1,2-Propanediol was used as the liquid medium for the isothermal bath. The bath temperature was varied over the range from 80 to 180°C. The total path length of the spinline through the LIB, or bath depth, was varied from 15 to 60 cm, or the maximum depth possible, which depended strongly on the LIB position, liquid temperature, and take-up velocity. The variation in liquid depth allowed for added control in both the amount of viscous drag imposed and the residence time within the bath experienced by the filament.

A liquid collector mounted directly under the bath in the spinline was used to recycle the liquid. More importantly, the use of the liquid collector allowed the threadline path to be made completely straight, thereby removing the undesirable bend present in the previous bath design. This vastly improved the high-speed spinning operability, especially during the operation of the LIB at higher temperatures and/or positions nearer to the spinneret. After passing through the bath, the filament was finally collected on a take-up godet at speeds varied from 3000 to 5000 m/min.

In this study, six sample series (A–F) were prepared when any of the four variables in the melt-spinning processing—LIB position, liquid temperature, liquid depth, and take-up velocity—were changed independently of the other three. Table I clearly shows each sample series and the conditions under which they were prepared. The series A, B, and C were produced to examine the effect of changes in take-up velocity, LIB temperature, and liquid depth, respectively. The series D and E were produced to examine the effect of changes in LIB position, at a constant LIB temperature and depth, for take-up velocities of 3000 and 4000 m/min, respectively. The F series was produced to examine the effect of using the maximum LIB depth at each LIB position, at a constant take-up velocity of 4000 m/min and LIB temperature of 140°C. The structural features and mechanical properties of such samples were compared.

Table I Preparation Conditions of Various Fibers

Sample ID	Take-up Velocity (m/min)	LIB Temperature (°C)	LIB Depth (cm)	LIB Position
A1	3000	140	22	3
A2	3500			
A3	4000			
A4	4500			
A5	5000			
B1	4000	86	28	3
B2		112		
B3		141		
B4		163		
B5		180		
C1	4000	140	10	3
C2			15	
C3			20	
C4			25	
C5			30	
C6			34	
D1	3000	140	22	0
D2				1
D3				2
D4				3
E1	4000	140	17	0
E2				1
E3				2
E4				3
F1	4000	140	17	0
F2			23	1
F3			37	2
F4			36	3

Structural Characterization and Mechanical Property Measurements

Birefringence

Birefringence measurements were made with a Leitz 20-order tilting compensator mounted in a Nikon polarizing microscope. A micrometer was also mounted in the microscope to determine fiber diameter. An average of five individual determinations was reported. The radial distribution of orientation was qualitatively evaluated through observation of

the parallel polarization interference patterns using a Jena interference microscope.

Density and Crystallinity

The volume fraction crystallinity was calculated from density values measured at 23°C in a sodium bromide density gradient column, using the following equation:

$$X_v = \frac{\rho - \rho_a}{\rho_c - \rho_a} \tag{2}$$

where ρ is the density of the fiber samples, and ρ_c and ρ_a, the densities of the crystalline and amorphous phases, respectively. In accord with the literature, values of 1.455 and 1.335 g/cm^3 were used for ρ_c and ρ_a, respectively.[17]

Analysis of Crystalline and Amorphous Structures

Wide-angle X-ray diffraction (WAXD) intensity curves for equatorial, meridional, and azimuthal scans were measured using a Siemens type-F X-ray diffractometer system. Nickel-filtered (λ = 0.1542 nm) CuKα radiation was used throughout all measurements. All the diffraction scans were resolved using the Pearson VII function.[18] The apparent crystal sizes L_{hkl} were calculated from the resolved peaks of the (010), ($\bar{1}$10), (100), and ($\bar{1}$05) reflections using the Scherrer equation[19]:

$$L_{hkl} = K\lambda/\{\beta \cos[(2\theta)/2]\} \tag{3}$$

where β is the width at half-height of reflection, K is taken to be 0.89, 2θ is the Bragg angle, and λ is the wavelength of the X-ray beam.

The degree of crystallite orientation, f_c, is defined as[20]

$$f_c = (3\langle\cos^2\phi_{c,z}\rangle - 1)/2 \tag{4}$$

where $\phi_{c,z}$ is the angle between the fiber axis and the c direction of the unit cell. $\phi_{c,z}$ can be related to $\phi_{\bar{1}05,z}$ from the knowledge of the angle α between the normal to plane ($\bar{1}$05) and the c direction[21]:

$$\langle\cos^2\phi_{c,z}\rangle = \langle\cos^2\phi_{\bar{1}05,z}\rangle/\cos^2\alpha \tag{5}$$

$$\langle\cos^2\phi_{\bar{1}05,z}\rangle = \left[\int_0^{\pi/2} I(\phi)\sin\phi\cos^2\phi\, d\phi\right] \Big/ \left[\int_0^{\pi/2} I(\phi)\sin\phi\, d\phi\right] \tag{6}$$

where $I(\phi)$ is the intensity of the resolved peak at the azimuthal angle ϕ.

The amorphous orientation factor (f_a) was determined from birefringence, the X-ray determined value of f_c, and density measurements using the following relation[22]:

$$f_a = \frac{\Delta n - X_v f_c \Delta n_c}{(1 - X_v)\Delta n_a} \tag{7}$$

The intrinsic birefringences of the crystalline and amorphous phases, Δn_c and Δn_a, were taken as 0.22 and 0.275 (Ref. 23), respectively.

The structural characteristics of fibers were also examined by infrared spectroscopy. The unpolarized infrared absorption spectra were recorded with a Nicolet 510P spectrophotometer. Fiber samples were carefully arranged in a parallel manner on a small metal frame so as to reduce the presence of air gaps or overlaps. The vibrational bands in the spectral region from 700 to 1100 cm^{-1} were fitted using the Pearson VII function, following the method introduced in Refs. 24 and 25.

Tensile Testing

Tensile testing was performed on an Instron machine Model 1122. Single filaments were tested using a gauge length of 25.4 mm and a constant crosshead speed of 20 mm/min. An average of five individual tensile determinations was reported for each sample.

RESULTS AND DISCUSSION

The Effect of Take-up Velocity on Structure and Properties

Figure 2 shows the take-up velocity dependencies of birefringence and density of the series A spun fibers. As listed in Table I, the series A samples were collected at take-up velocities ranging from 3000 to 5000 m/min, with the LIB fixed at position 3, and the liquid depth and temperature held constant at 22 cm and 140°C, respectively. For comparison, data for high-speed spinning samples produced under normal cooling conditions (without any threadline modification) are also presented in Figure 2. Similar to the normal cooling spinning, the birefringence of sample series A shows a monotonical increase with increasing take-up velocity. It is quite clear that the birefringence in the series A samples is much higher than those of normal cooling samples at each take-up velocity. For example, at 4000 m/min take-up velocity, the birefringence of the LIB spun fiber is

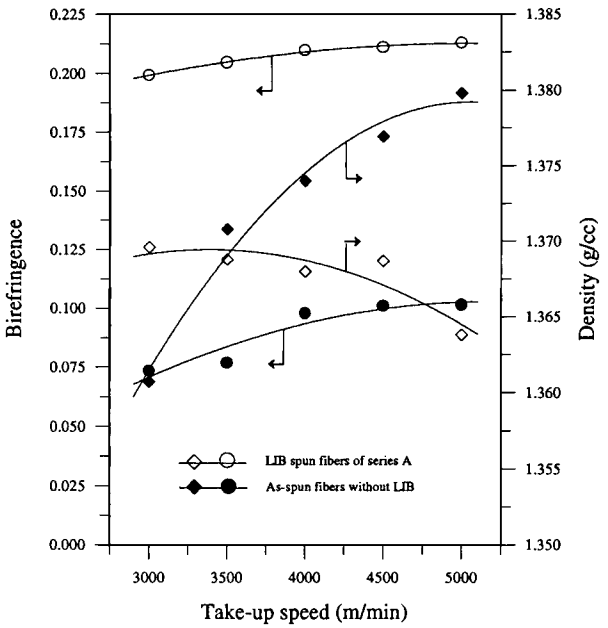

Figure 2 Effects of take-up velocity on birefringence and density of the series A LIB spun fibers and a normal cooling spun fiber (without LIB).

approximately twice as high as that of the normal cooling spun fiber, even though the LIB depth is only 22 cm and the residence time of the fiber passing through the liquid is very short. (An exact determination of this residence time would require a threadline velocity profile within the bath. Unfortunately, current limitations associated with the design and operation of the LIB have hindered the generation of threadline profiles; however, future efforts will be focused on their accurate measurement and/or calculation.) This suggests that the presence of the LIB had a dramatic impact on the development of threadline tension.

On the other hand, the take-up velocity dependence of the density between the series A and normal cooling samples shows a quite different trend. Although the normal cooling spun fibers show the expected monotonical increase in density over the range investigated, the density of the LIB spun fibers does not change significantly with increasing take-up velocity over the range from 3000 to 4500 m/min and then starts to decrease as the velocity is increased further to 5000 m/min. Figure 3 shows the X-ray diffraction scans of samples A1–A5. In spite of slightly better-resolved patterns appearing in the equatorial and azimuthal scans of sample A5, no obvious difference was observed among the five samples. The calculated apparent crystallite sizes and crystalline orientation factor, therefore, are almost the same for each of the series A samples. These results suggest that high threadline tension built up in the LIB can aid in the extension of mo-

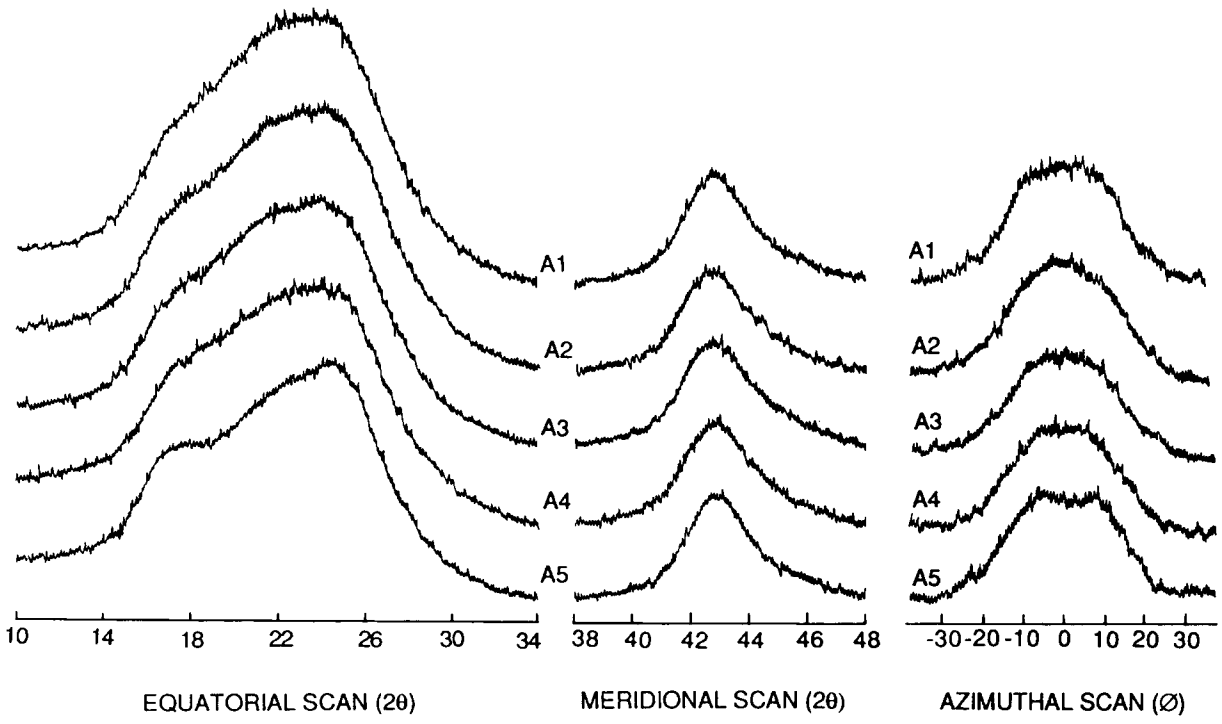

Figure 3 Equatorial, meridional, and azimuthal X-ray diffraction profiles of the series A fiber samples.

lecular chains, but it may be incapable of promoting the crystallization process.

It is common knowledge that the birefringence in the as-spun fibers is proportional to the threadline stress, which is influenced significantly by the aerodynamic drag force in the case of a normal cooling high-speed spinning process.[26] In our case, however, the threadline stress is primarily determined by the liquid drag applied on the filament as it passes through the LIB, and because the frictional drag in the liquid is several hundred times larger than that in the air,[27] the air drag contribution can be considered negligible. Based on the general principles of fluid mechanics, the frictional drag applied on a filament that passes through a liquid can be evaluated by the following equation:[28]

$$F = \int_0^D 2\pi\eta(dv/dr)|_{r=R}R(D)\,dD \qquad (8)$$

where F is frictional drag; η, viscosity of the liquid; $(dv/dr)|_{r=R}$, the velocity at the filament surface; $R(D)$, the radius profile function of filament in the LIB; and D, the liquid depth. The frictional drag can be considered to be proportional to η, $(dv/dr)|_{r=R}$, and D. Although, as previously stated, the physical presence of the bath limits our ability to collect quantitative information about the radius profile or velocity gradient within the bath, it is clear that $(dv/dr)|_{r=R}$ will be greater with increasing relative speed at the interface between the filament and fluid medium. Therefore, an increase in frictional drag with increasing take-up velocity resulting in an increase in the birefringence is a reasonable result.

The dependence of density on take-up velocity for the LIB spun fibers, however, is quite different. Such a phenomenon that the density of the as-spun fiber decreases after a certain critical velocity has been pointed out and discussed previously.[14] The degree of crystallinity (or density) in the as-spun fiber is determined by the product of crystallization time and crystallization rate, for a given level of orientation. Increasing the take-up velocity tends to increase the threadline tension and may increase the crystallization rate through a higher level of orientation, but the crystallization time is always decreasing. Assuming comparable levels of orientation, at a certain critical velocity, the product of crystallization rate and crystallization time reaches a maximum. As a result, further increases in take-up velocity reduce the time available for crystallization to occur and results in the reduction of density. Normally, the growth rate of crystallization is accelerated by higher threadline stress. However, this may not always be the case. When extremely high threadline tension is induced by higher take-up velocity and/or greater depth of the liquid bath (as represented later), molecular chains may be tautly strained and rendered less mobile. The growth of crystals may thus be restricted, which may also contribute to the observed reduction in density.

Fiber tenacity, initial modulus, and elongation at break of samples A1–A5 are plotted in Figure 4 as a function of take-up velocity. Similar to the trend observed for birefringence, the tenacity and modulus of the as-spun fibers increase almost linearly with take-up velocity, while the elongation is very low and remains essentially constant for take-up velocities greater than or equal to 3500 m/min.

The Effect of Liquid Temperature on Structure and Properties

Series B was prepared in order to examine the structural and mechanical property dependencies on the LIB temperature, whereas the other variables

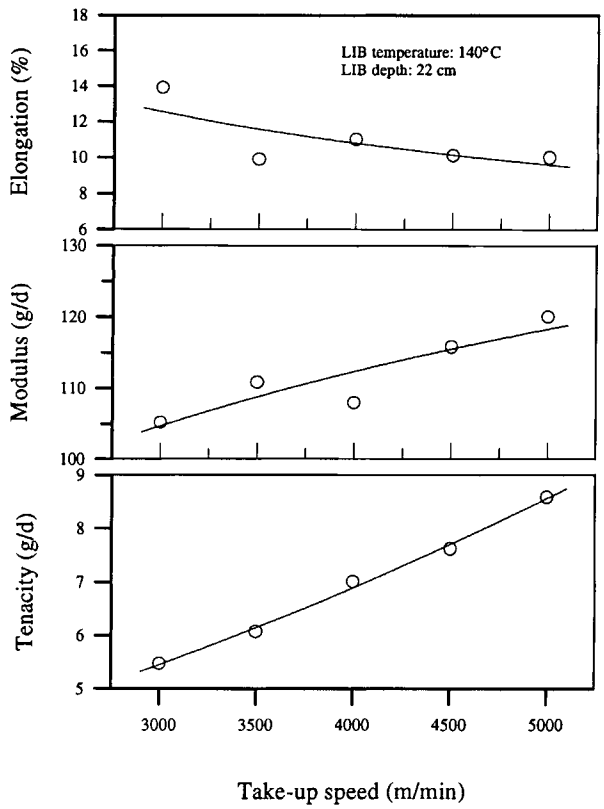

Figure 4 Effect of take-up velocity on mechanical properties of the series A LIB spun fibers.

Table II Structural Analysis and Mechanical Properties of LIB Spun Fibers with Different LIB Temperatures

Sample ID	LIB Temp (°C)	Apparent Crystallite Size (nm)				Density (g/cc)	Δn	f_c	f_a	Tenacity (gf/d)	Modulus (gf/d)	Elongation (%)
		L_{100}	$L_{\bar{1}10}$	L_{010}	$L_{\bar{1}05}$							
B1	86	1.86	1.21	1.10	2.35	1.359	0.201	0.84	0.74	6.01	92.5	18.5
B2	112	2.10	1.32	1.23	2.57	1.354	0.209	0.87	0.77	7.09	103.1	11.1
B3	141	2.42	1.60	1.56	3.12	1.368	0.212	0.89	0.79	7.95	109.3	10.1
B4	163	3.35	1.80	1.99	3.45	1.373	0.210	0.91	0.78	7.81	119.7	10.0
B5	180	3.80	3.39	2.11	3.74	1.375	0.207	0.92	0.76	7.41	111.8	10.1

were held constant (take-up velocity = 4000 m/min, LIB fixed at position 3, and liquid depth = 28 cm). As shown in Table II, apparent crystallite size (L_{010}, $L_{\bar{1}10}$, L_{100}, and $L_{\bar{1}05}$), specimen density ρ, and crystalline orientation factor, f_c, increase rapidly with increasing liquid temperature. The specimen birefringence, amorphous orientation factor, and tenacity, however, show a maximum within a temperature range around 140°–160°C.

It is well recognized that crystallization and molecular orientation are controlled largely by the combined interaction of threadline temperature, threadline stress, and time. However, use of the LIB appears to separate the behavior of crystallization and molecular orientation from the combined effects of threadline temperature and threadline stress. In other words, crystallization depends mainly on the temperature change, whereas the orientation, in particular within the amorphous regions, depends mainly on the threadline stress. In a certain temperature range below T_m, chain segment mobility and molecular deformability were activated by the increasing temperature, resulting in the encouragement of crystal growth and orientation. At the same time, however, the viscosity of the liquid bath medium decreases gradually with increasing temperature. Figure 5 shows the temperature dependence of the viscosity of 1,2-propanediol. For example, when the liquid temperature was raised from 120 to 160°C, the viscosity drops about 25%. As shown in eq. (8), the reduction of viscosity will decrease the frictional drag acting on the filament surface. Therefore, as the temperature increases, the drag imposed by the liquid becomes less, with a corresponding reduction in threadline stress. Also, a higher filament temperature would lead to shorter relaxation times of the constituent chains. The combined effects of reduced threadline tension and shorter relaxation times results in a lower level of amorphous orientation. The existence of such a critical temperature may be the main cause for the appearance of the maximum in the birefringence, amorphous orientation, and fiber tenacity.

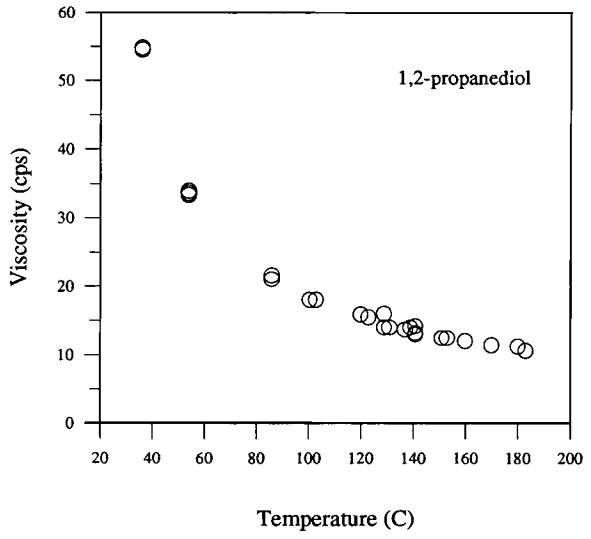

Figure 5 Effect of temperature on viscosity of liquid medium.

The Effect of Liquid Depth on Structure and Properties

Figures 6 and 7 show the structural and mechanical property dependencies on liquid depth, respectively, for the series C samples. Note that for the series C samples the take-up speed, LIB position, and liquid temperature were fixed (refer to Table I). Birefringence, amorphous orientation, tenacity, and modulus of the spun fibers increase steadily with increasing liquid depth. However, the crystallinity and crystallite orientation show a maximum at a liquid

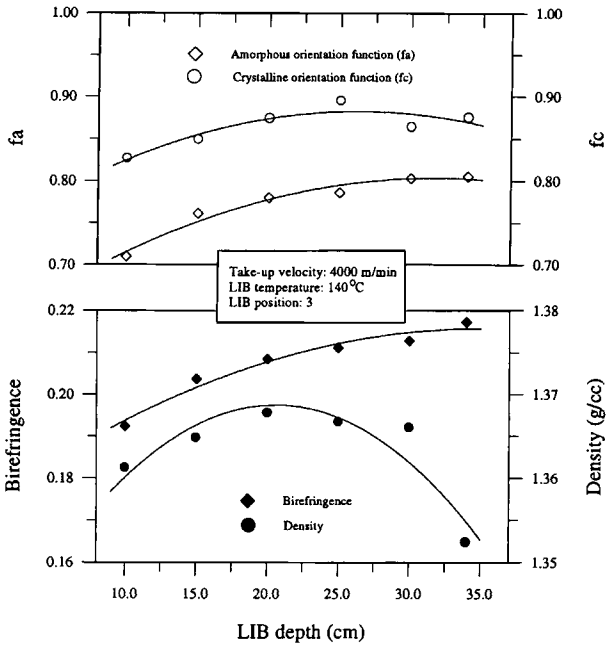

Figure 6 Effects of LIB depth on birefringence, density, and orientation factors of the series C LIB spun fibers under indicated conditions.

depth of approximately 20–25 cm. As mentioned above, an increase in liquid depth increases the amount of frictional drag and resulting threadline stress, thereby inducing greater molecular orientation. This greater level of orientation would presumably increase the rate of crystallization; however, the extremely high tension present is believed to limit segmental motion of the molecular chains and thereby retard the crystalline growth process. Although this extremely high tension may retard crystallization, it also results in a significant proportion of chains being maintained in an extended state, leading to the observed superior mechanical properties.

The Effect of LIB Position on Structure and Properties

To study the effect of the LIB position on structural and mechanical properties of as-spun fibers, the LIB was positioned vertically along the spinline over a relatively wide range of positions or distances from the spinneret. The original purpose of moving the LIB closer to the spinneret was to study whether the molecular relaxation process in the molten region could be minimized by controlling the threadline tension and temperature in this critical region of structure development. In this study, the air gap (distance between spinneret and top of liquid surface) could be narrowed to within only 3–5 cm, when using a take-up velocity of 3000 m/min, an LIB temperature of 140°C, and a depth of approximately 20 cm. However, the spinning operability for this particular set of conditions was poor. Therefore, the top LIB position in the spinline (designated position 0) was located such that the bottom of the bath was 30 cm from the spinneret face. The distance between the spinneret and the liquid surface in this case was about 10 cm. Although the threadline in this region appears to be very weak, it was proved that the extrudate could endure the high frictional drag without breakage.

The key difference between the series E and F samples was that the LIB depth in the former was kept at 17 cm, whereas in the latter, the LIB depth was maintained as large as possible without threadline rupture occurring. Note that the take-up velocity and the LIB temperature remained at 4000 m/min and 140°C, respectively, for all the series E and F samples. The effect of the LIB position on the radial variation of structure in the fiber series E and F was studied using a Jena interference microscope.

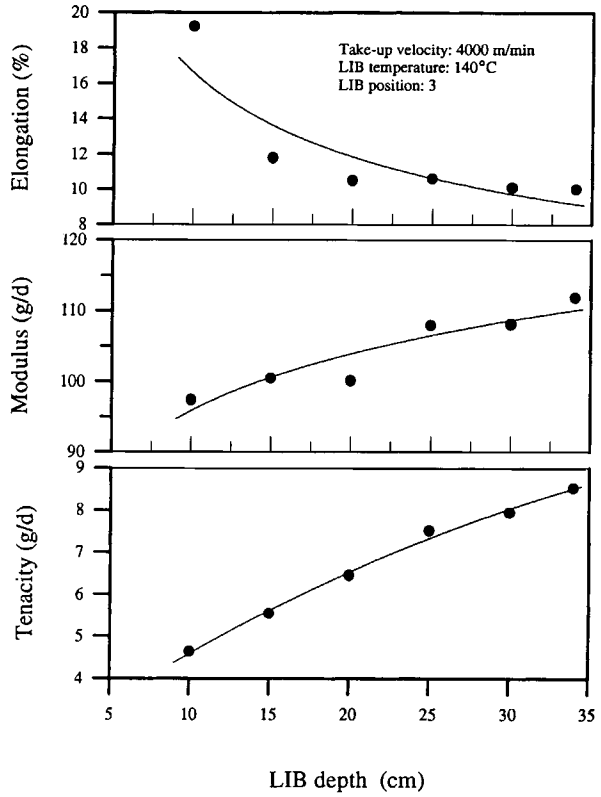

Figure 7 Effect of LIB depth on mechanical properties of the series C LIB spun fibers.

Since little variation was observed in the refractive index profile in the direction perpendicular to the fiber axis, observation of a single parallel polarization interference photograph for each sample provides a good indication of the presence of radial variation. Figure 8 shows the parallel polarization interference patterns of the four series F samples (F1–F4). It is quite evident that fiber samples spun from LIB 0 and LIB 1 show a skin–core structure variation, with birefringence at the fiber core being relatively lower. Such structural difference is most distinct in the LIB 0 spun fiber. However, a uniform radial structure was observed in the spun fibers produced using LIB positions 2 and 3, with all other process parameters being held constant. For series E, the same LIB position-dependent structures were observed, where a skin–core structure was present in samples E1 and E2, whereas E3 and E4 had uniform structures. This skin–core structure was present only in the fiber samples produced at the LIB 0 and LIB 1 positions. Note that this same type of characterization was also performed on sample series A, B, and C. A uniform parallel polarization interference pattern was observed for each of those 16 samples. All the samples within series A, B, and C were prepared under quite different conditions in liquid depth, temperature, and take-up velocity; however, all these samples were prepared using the

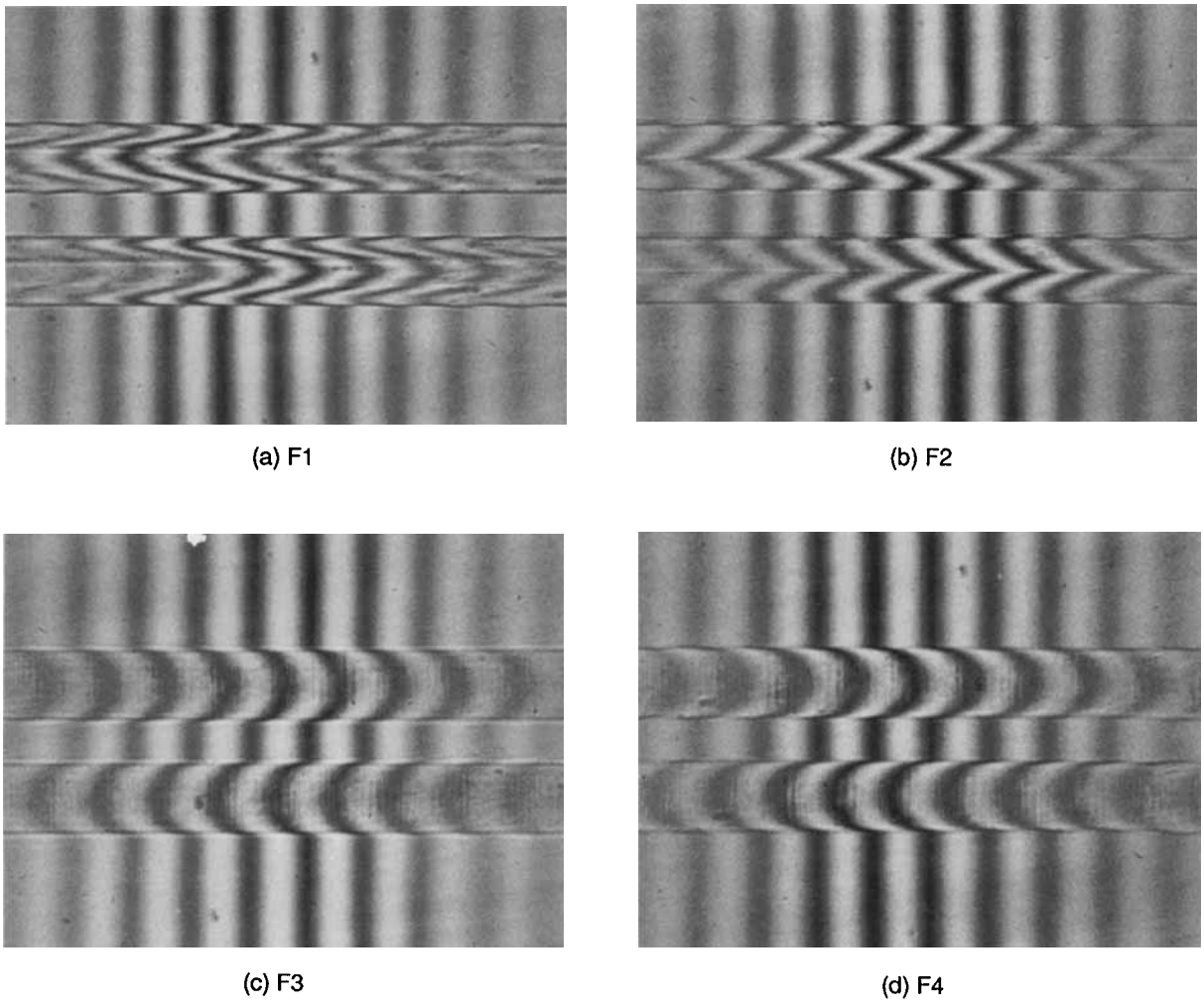

Figure 8 Parallel polarization interference patterns of the series F LIB spun fibers under different LIB conditions: (a) 4000 m/min take-up with LIB position 0 (140°C and 17 cm); (b) 4000 m/min take-up with LIB position 1 (140°C and 22 cm); (c) 4000 m/min take-up with LIB position 2 (140°C and 37 cm); (d) 4000 m/min take-up with LIB position 3 (140°C and 36 cm).

same LIB position (LIB 3). This fact suggests that the state of extrudate before entering the LIB strongly influences the radial uniformity of the resulting structure. If the threadline had more nearly solidified before entering the LIB, as believed to be the case for positions 2 and 3, the resultant fiber had a uniform radial structure, regardless of the LIB temperature and depth.

Figure 9 shows X-ray diffraction scans of the equatorial, meridional, and azimuthal profiles for samples E1–E4 and a normal cooling sample obtained at a 4000 m/min take-up velocity for comparison. As the LIB position was moved closer to the spinneret, the equatorial diffraction scan became gradually more well resolved, indicating a more highly developed crystalline structure. The individual equatorial diffraction peaks are only distinguishable in the LIB 0, LIB 1, and normal cooling spun fibers, indicating that crystal growth was significant in each of these three samples. As for the spun fiber samples produced using LIB positions 2 and 3, the crystal growth process appears to have been restricted. At the same time, the width at half-height of reflection peaks in the meridional profile gradually became narrower as the LIB was moved closer to the spinneret face. In the azimuthal profiles, distinct peak separation begins to occur as the LIB was moved closer to the spinneret, indicative of a higher degree of crystallite orientation.

Figure 10 shows X-ray diffraction scans of the equatorial, meridional and azimuthal profiles for samples F1–F4 and a commercial tire cord yarn produced by a traditional two-step spin-draw process for comparison. Diffraction scans of the tire cord show a well-developed crystalline structure. In this case, only the fibers spun using the LIB 0 position show well-resolved diffraction peaks. Also worthy of noting is the obvious difference between equatorial profiles of the samples E2 and F2. Although three individual diffraction peaks can be clearly recognized in the E2 fiber sample, the F2 fiber sample has a poorly resolved pattern with mutually overlapping diffraction peaks. The only difference in the preparation of these samples was the LIB depth, which was 17 and 23 cm for samples E2 and F2, respectively, a difference of only 6 cm. This dependence of crystalline development on LIB depth for LIB position 1 appears to be even stronger than that

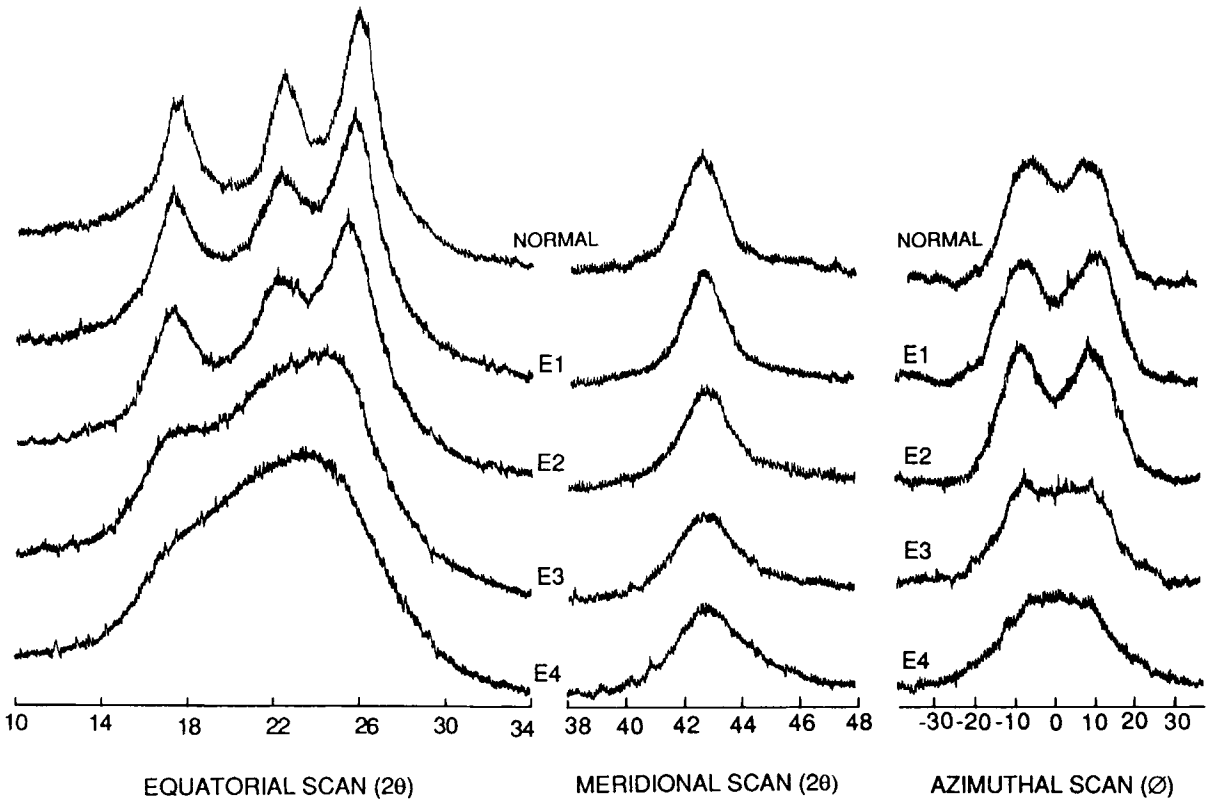

Figure 9 Equatorial, meridional, and azimuthal X-ray diffraction profiles of the series E LIB spun fibers and a normal cooling spun fiber.

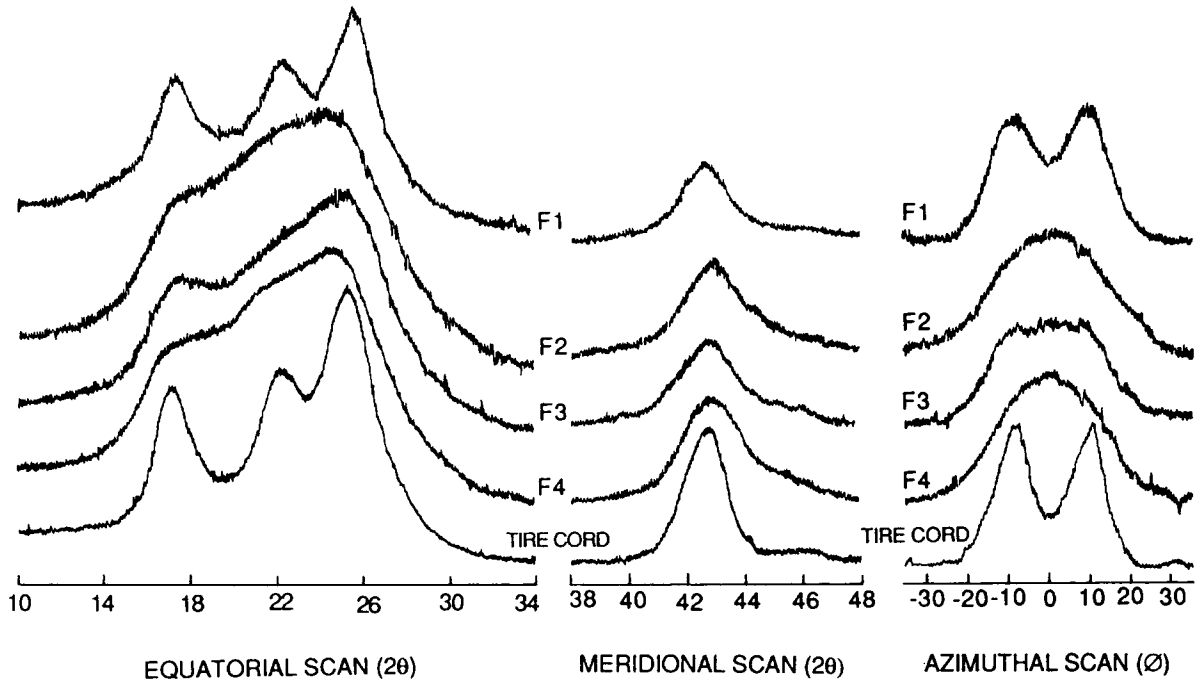

Figure 10 Equatorial, meridional, and azimuthal X-ray diffraction profiles of the series F LIB spun fibers and a commercial tire cord yarn.

observed for LIB position 3, as in the series C fiber samples.

The apparent crystallite sizes and crystalline orientation factor calculated from X-ray diffraction patterns are presented and compared with the amorphous orientation factor and mechanical properties in Table III for series D, E, and F. The apparent crystallite sizes and crystalline orientation factor achieved using LIB positions 0 and 1 are significantly higher than those achieved using LIB po-

Table III Structural Analysis and Mechanical Properties of LIB Spun Fibers with Different LIB Positions

Sample ID	LIB Position	Apparent Crystallite Size (nm)				Density (g/cc)	Cryst (Vol %)	Δn	f_c	f_a	Tenacity (gf/d)	Modulus (gf/d)	Elongation (%)
		L_{100}	$L_{\bar{1}10}$	L_{010}	$L_{\bar{1}05}$								
D1	0	3.30	2.99	2.67	3.73	1.364	0.24	0.099	0.91	0.24	3.39	77.1	13.4
D2	1	2.71	2.75	2.14	3.61	1.386	0.27	0.170	0.91	0.58	5.33	96.1	26.2
D3	2	2.13	1.70	1.44	3.10	1.367	0.26	0.205	0.88	0.76	5.82	101.1	13.5
D4	3	1.98	1.44	1.38	2.67	1.368	0.28	0.205	0.87	0.77	5.72	107.0	17.3
E1	0	3.58	3.23	3.08	4.59	1.367	0.26	0.110	0.94	0.28	4.10	84.6	13.0
E2	1	3.37	3.14	2.68	4.38	1.372	0.31	0.161	0.93	0.51	4.91	96.8	19.4
E3	2	2.91	1.90	1.77	3.46	1.367	0.26	0.190	0.92	0.67	5.66	101.3	15.2
E4	3	1.96	1.38	1.50	3.04	1.368	0.27	0.205	0.88	0.76	5.88	105.9	12.3
F1	0	3.58	3.23	3.08	4.59	1.367	0.26	0.110	0.94	0.28	4.10	84.6	13.0
F2	1	2.10	2.04	1.47	3.24	1.368	0.28	0.176	0.91	0.61	6.59	82.7	25.4
F3	2	2.63	2.01	1.82	3.70	1.355	0.17	0.220	0.92	0.82	9.41	112.4	10.1
F4	3	2.50	2.07	1.53	3.10	1.360	0.21	0.216	0.91	0.80	8.83	93.6	11.7
Tire yarn	—	4.52	3.95	3.05	3.10	1.391	0.47	0.216	0.94	0.82	9.03	104.3	16.9

sitions 2 and 3. Because the LIB positions 0 or 1 are relatively close to the spinneret, the extrudate entering the LIB at position 0 or 1 is considered to be molten or semimolten and to have a relatively large diameter, low velocity, and low viscosity. The initial imposed frictional drag and resulting threadline tension are also low. Thus, there will be relatively higher molecular mobility and sufficient time to promote the crystallization growth process. This line of reasoning is substantiated by the observed trends in crystallite sizes stated previously. As for the LIB positions 2 and 3, it is believed that the threadline diameter is gradually reduced and that the threadline velocity reaches a much higher level before the filament enters the LIB. As discussed previously, in accord with eq. (8), a higher threadline velocity within the LIB will create a higher frictional drag and result in a very high threadline tension. This high threadline tension may be straining molecular chains to the extent that segmental motion is restricted and the crystallization process thereby diminished. The enhanced straining of molecular chains has resulted in higher birefringence, higher amorphous orientation, and higher mechanical properties. The diminished crystallization process, however, has resulted in smaller crystallite sizes as shown in Table III. Although the apparent crystallite sizes decrease significantly when the LIB is moved to a lower position, the crystallinities observed in such samples are nearly equivalent.

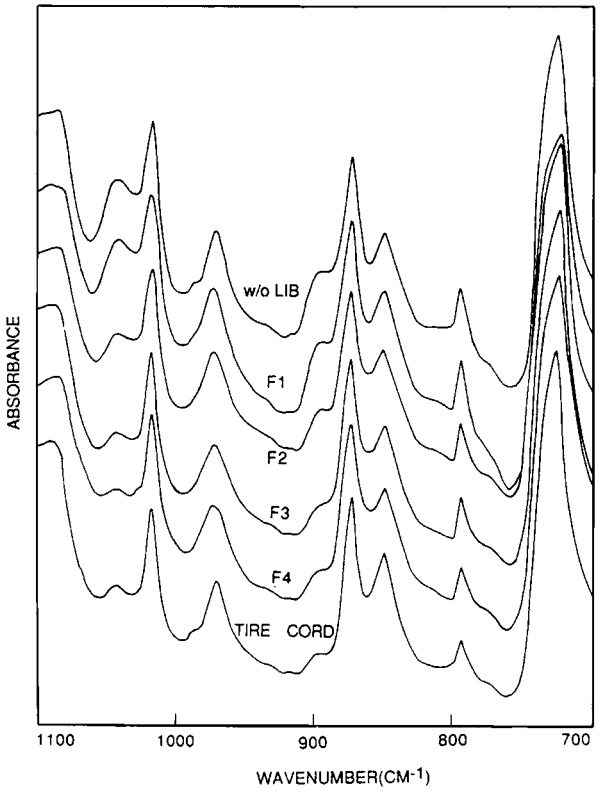

Figure 11 Unpolarized infrared spectra of the series F LIB spun fibers and both the normal cooling spun fiber and the commercial tire cord yarn.

Table IV Dependence of Absorbance Ratio A_{899}/A_{845} on the Sample Preparation Condition

Sample ID	A_{899}/A_{845}
Normal Cooling (without LIB)	0.30
F1	0.31
F2	0.18
F3	0.13
F4	0.13
Tire yarn	0.12

The structural features of different samples were also studied using infrared spectroscopy. The unpolarized infrared spectrum, over the wavenumber region 700–1100 cm^{-1}, of series F samples are shown in Figure 11. The measured spectrum for the normal cooling spun fiber at take-up speed 4000 m/min and the tire cord yarn are also presented in this figure for comparison. A primary molecular deformation mechanism is considered to be the *gauche–trans* transition that typically occurs when a PET filament is elongated. Differences in the relative amounts of a particular molecular conformation present in a fiber sample can be evaluated by properly fitting the spectrum with the necessary absorbance bands and calculating the ratio of areas between the appropriate bands.[5,6,24,25] The presence of *gauche* conformers in a PET chain is indicative of portions of a molecule that are not straight, whereas the presence of *trans* conformers in a PET chain is indicative of portions of the molecule that are straight. However, the presence of a high *trans* content in an unpolarized spectrum does not necessarily imply how the molecules are aligned with respect to the fiber axis: only that the molecules are relatively straighter. Note that the interior region of the crystalline phase must contain only *trans* conformations. For PET, the 899 and 1043 cm^{-1} bands are assigned to the amorphous *gauche* conformers, and the 845 and 970 cm^{-1} bands are assigned to the combined crystalline and amorphous *trans* conformers.[24]

The observed infrared absorption ratio A_{899}/A_{845} for the above six samples are listed in Table IV. A low value of such a ratio can be considered indicative of a relatively high percentage of *trans* conformations being present in a given sample. From these

data, the six samples can be divided into two groups: One group includes the normal cooling high-speed spun fiber and the fiber spun using LIB position 0. They have a high *gauche* conformer content and are characterized by low amorphous orientation, which results in the observed low mechanical properties. The other group includes the fibers spun using LIB positions 1, 2, and 3, as well as the commercial tire cord yarn, the common feature being that they all have comparably high *trans* conformer contents. However, when the comparable ratio of *gauch*-to-*trans* conformers present in the fiber samples produced using the LIB positions 1, 2, and 3 are considered in conjunction with the high level of overall orientation (Δn) and low level of crystallinity, the conclusion emerges that the amorphous orientation should be higher in the LIB spun fiber samples than in the tire cord yarn. This finding is in good agreement with the previously discussed amorphous orientation factors.

Figure 12 shows the stress–strain curves for the series F samples (F1–F4); the previous normal cooling high-speed spun fiber and the commercial tire cord yarn are also shown. All the series F samples and the high-speed spun fiber were produced at a take-up velocity of 4000 m/min. The tenacity and initial modulus in the normal cooling fiber were very low at this take-up speed. As expected, fibers taken from the tire cord yarn displayed both a high modulus and tenacity. As shown, the spun fibers prepared using LIB positions 0 and 1 exhibit an obvious second yield point, where the stress reaches a plateau region as the elongation increases. The LIB 0 and LIB 1 spun fibers also possess a relatively low te-

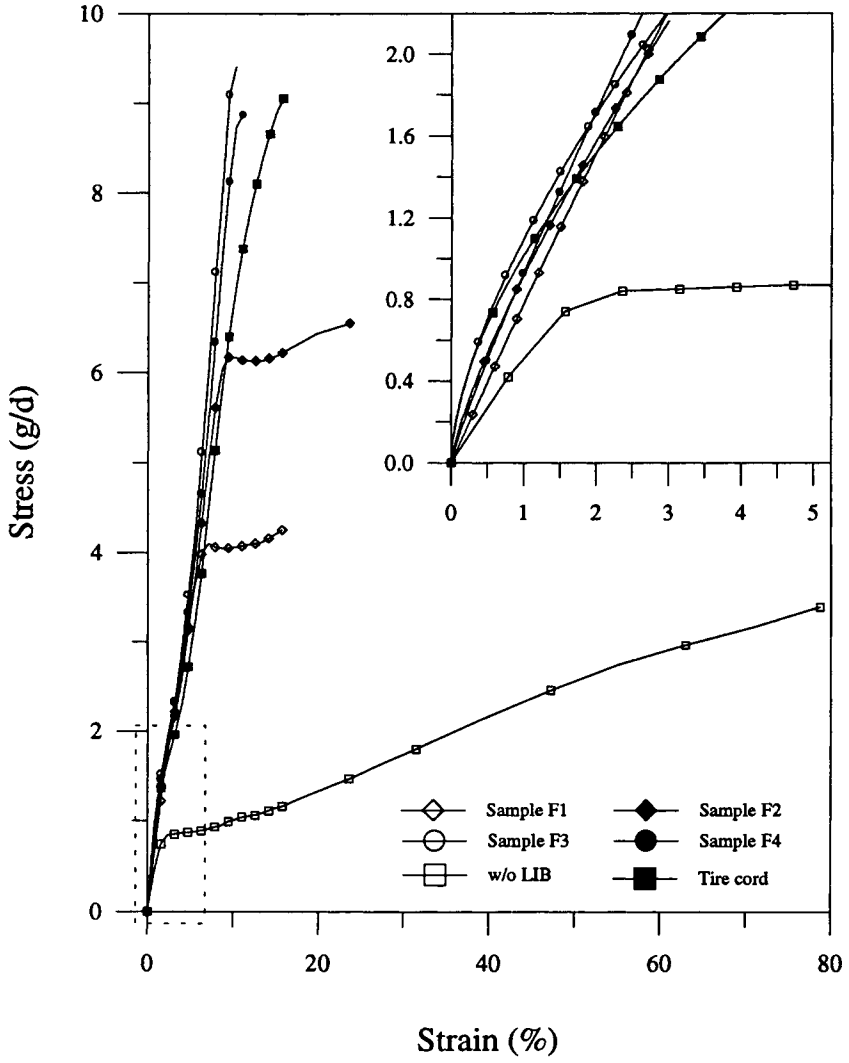

Figure 12 Stress–strain curves of the series F LIB spun fibers and both the normal cooling spun fiber and the tire cord yarn.

nacity and high modulus. The poor yield resistance and low tenacity of these samples are consistent with their relatively lower values of birefringence and amorphous orientation as listed in Table III. Although the initial (low strain) mechanical behavior of the spun fibers prepared using LIB positions 2 and 3 (F3 and F4) was similar to the previous fibers (F1 and F2), the higher strain behavior was quite different. Although the F3 and F4 spun fibers have a low crystallinity, their tenacities are as high as, or greater than, that of the commercial tire cord. These results are attributed to the extremely high amorphous orientation and provide further support that amorphous orientation is crucial in the development of superior mechanical properties. The above stress–strain behavior was also observed for other sample series in which the only preparation difference was the use of take-up velocities of 3000 and 5000 m/min, with similar conclusions being drawn in each case.

Figures 13 shows the relationship between fiber birefringence and tenacity. The birefringence and tenacity values for all of the samples prepared under various LIB conditions and take-up speeds are shown in this figure. In each case, the birefringence was shown to increase as the LIB was moved further from the spinneret. As would be expected, the tenacity increased as the birefringence increased. The spun fibers prepared using LIB positions 2 and 3 have high birefringence and high tenacity, with a few exceptions, where low liquid temperatures were used. In general, the tenacity of all the samples produced in this study (series A–F) was found to correlate strongly with the measured mean birefringence.

CONCLUSIONS

The melt-spinning of PET filaments was modified through the use of a liquid isothermal bath (LIB) in the spinline. Several process variables, including take-up velocity, LIB position, LIB depth, and LIB temperature, were experimentally varied. The effects of such changes on the structure and mechanical properties of as-spun fibers were studied.

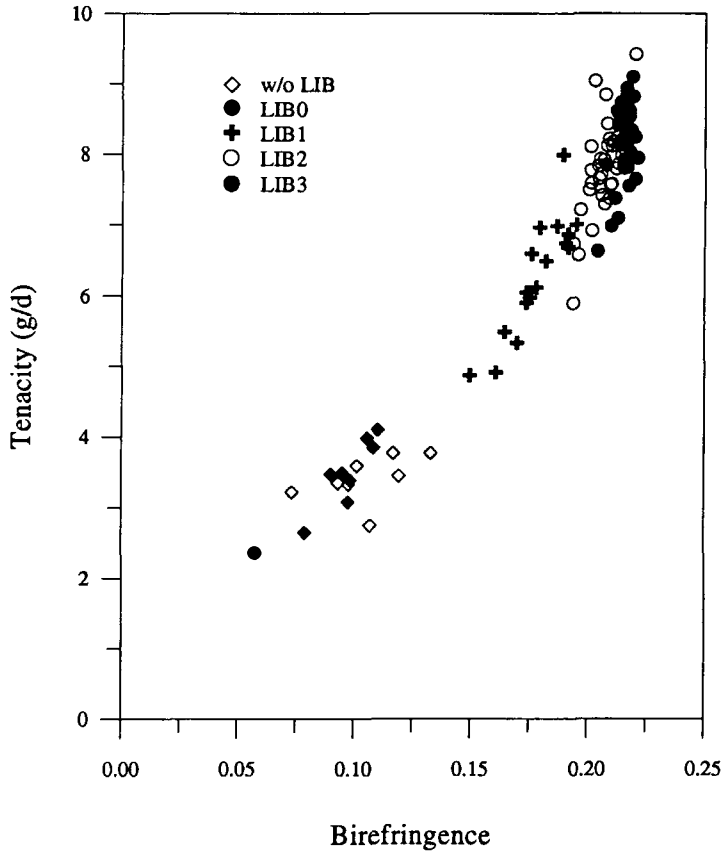

Figure 13 Tenacity vs. birefringence for LIB spun fibers produced at various LIB positions; the normal cooling spun fiber is also shown.

The following observations were made when the LIB was used at a position relatively distant from the spinneret (LIB 3). Increases in take-up velocity, LIB temperature, and LIB depth usually resulted in monotonical increases in apparent crystallite sizes, fiber birefringence, and mechanical properties. A high LIB temperature induced a significant increase in sample crystallinity. However, use of an extremely high take-up velocity and great LIB depth induced a significant reduction in sample crystallinity. This reduction in crystalline growth is believed to occur due to a restriction in chain segment mobility, which, in turn, is attributed to the extremely high threadline tension developed within the bath. Although this high threadline tension may reduce the crystalline growth process, it also allows for molecular chains to be stretched and maintained in an extended state until solidification occurs. The presence of such extended chain material in the solidified filament would undoubtedly support the excellent mechanical properties observed in these spun fiber samples.

When the LIB was moved to a position relatively closer to the spinneret (LIB 0 and 1), apparent crystallite sizes increased significantly, whereas the overall sample crystallinity remained nearly constant. This phenomenon was considered to be a result of the higher threadline temperature and high chain segment mobility present within the semimolten extrudate for LIB positions 0 and 1. The purpose of moving the liquid bath close to the spinneret was to study whether molecular relaxation could be restricted by controlling the threadline tension and temperature in this critical region of structure development. Although the threadline in this region appears to be very weak, it was proved that the extrudate can endure the high frictional drag imposed by the LIB without breakage. However, as previously stated, the threadline tension developed in this region is believed to be much lower than that of LIB positions 2 and 3. As a result, samples prepared using the LIB 0 position had a relatively low birefringence, tenacity, and modulus when compared with samples prepared using LIB positions further from the spinneret.

In the wide temperature and take-up velocity ranges investigated, samples obtained from both LIB positions 2 and 3 have similar mechanical properties. The most suitable LIB temperature range seems to be 130–160°C, with a take-up velocity of 3500–4500 m/min. Most of the samples obtained under such conditions possess a high tenacity, high modulus, and low elongation. Characterization of these unique fiber samples has also revealed the presence of low crystallinity and high amorphous orientation.

REFERENCES

1. A. Ziabicki, *Fundamentals of Fiber Formation,* Wiley, London, 1976.
2. R. J. Samuels, *Structured Polymer Properties,* Wiley-Interscience, New York, 1973.
3. J. Shimizu, K. Toriumi, and Y. Imai, *Sen-i Gakkaishi,* **33,** T-255 (1977).
4. H. M. Heuvel and R. Huisman, *J. Appl. Polym. Sci.,* **22,** 2229 (1978).
5. T. Kunugi, A. Suzuki, and M. Hashimoto, *J. Appl. Polym. Sci.,* **26,** 213 (1981).
6. T. Kunugi, A. Suzuki, and M. Hashimoto, *J. Appl. Polym. Sci.,* **26,** 1951 (1981).
7. J. H. Southern and R. S. Porter, *Am. Chem. Soc. Polym. Prepr.,* **10,** 1028 (1969).
8. J. H. Southern and R. S. Porter, *J. Macromol. Sci.-Phys.,* **B4,** 541 (1970).
9. M. Ito, K. Tanaka, and T. Kanamoto, *J. Polym. Sci. Polym. Phys. Ed.,* **25,** 2127 (1987).
10. M. Ito, K. Takahashi, and T. Kanamoto, *J. Appl. Polym. Sci.,* **40,** 1257 (1990).
11. J. Shimizu, K. Toriumi, and K. Tamai, *Sen-i Gakkaishi,* **33,** T-208 (1977).
12. J. Shimizu, N. Okui, and T. Kikutani, *Sen-i Gakkaishi,* **37,** T-135 (1981).
13. R. Huisman and H. M. Heuvel, *J. Appl. Polym. Sci.,* **37,** 595 (1989).
14. J. A. Cuculo, P. A. Tucker, and G. Y. Chen, *J. Appl. Polym. Sci. Appl. Polym. Symp.,* **47,** 223 (1991).
15. C. Y. Lin, P. A. Tucker, and J. A. Cuculo, *J. Appl. Polym. Sci.,* **46,** 531 (1992).
16. A. Conix, *Makromol. Chem.,* **26,** 226 (1958).
17. R. P. Daubeny, C. W. Bunn, and C. J. Brown, *Proc. R. Soc. Lond. A.,* **225,** 531 (1954).
18. H. M. Heuvel, R. Huisman, and K. C. J. B. Lind, *J. Polym. Sci. Polym. Phys. Ed.,* **14,** 921 (1976).
19. P. Scherrer, *Gottingher Nachrichten,* **2,** 98 (1918).
20. P. H. Herman, *Physics and Chemistry of Cellulose Fibers,* Elsevier, Amsterdam, 1949.
21. V. B. Gupta and S. Kumar, *J. Polym. Sci. Polym. Phys. Ed.,* **17,** 179 (1979).
22. R. S. Stein and F. H. Norris, *J. Polym. Sci.,* **21,** 381 (1956).
23. J. H. Dumbleton, *J. Polym. Sci. A-2,* 795 (1968).
24. H. M. Heuvel and R. Huisman, *J. Appl. Polym. Sci.,* **30,** 3069 (1985).
25. R. Huisman and H. M. Heuvel, *J. Appl. Polym. Sci.,* **37,** 595 (1989).
26. K. Fujimoto, K. Iohara, S. Owaki, and Y. Murase, *Sen-i Gakkaisgi,* **44,** 477 (1988).
27. T. Kikutani, H. Morinaga, A. Takaku, and J. Shimizu, *Int. Polym. Proc.,* **5,** 20 (1990).
28. A. Ziabicki, *Fundamentals of Fiber Formation,* Wiley, London, 1976, Chap. 4.

Received February 14, 1994
Accepted June 13, 1994